Chapter 6.

Active Imaging Sensors

6.1. Imaging Techniques

The two time-of-flight imaging techniques that are commonly used are as follows:

- 1D line scanner with forward velocity to produce a push-broom raster scan
- 2D scanner with orthogonal scan axes

6.1.1. Push Broom Scanner

A rotating prism scans the laser (or radar) beam at right angles to the direction of travel. The laser produces between 2000 and 8000 pulses every second. Each pulse strikes the ground and because it is rough, some power is reflected back to the receiver where it is detected. By registering the forward motion of the aircraft using GPS/INS and the beam angle, a 2D raster is produced as shown in the figure below. Range and /or reflected signal amplitude are logged to produce an image of the ground.

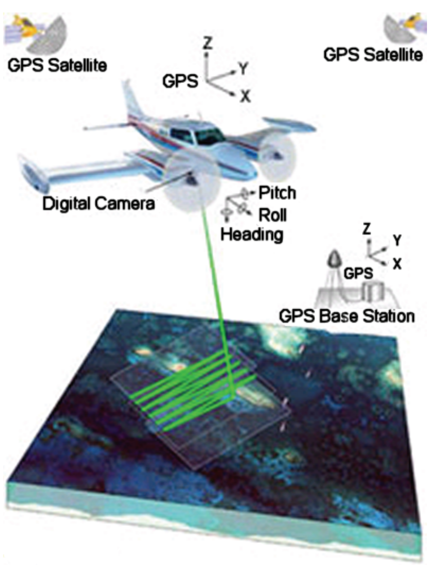

(a)

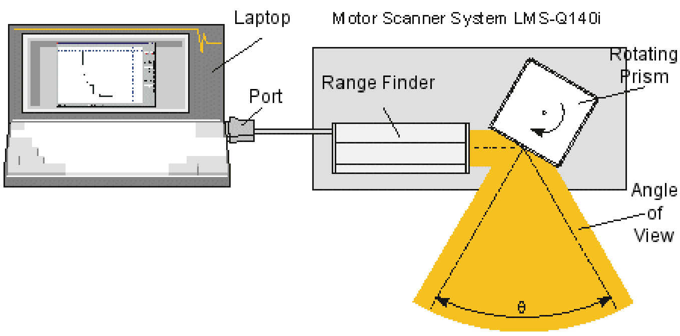

(b)

Figure 6.1: Push broom scan principles showing (a) generation of a raster image and (b) rotating prism mechanism to produce the scanned beam

6.1.2. 2D Scan Principles

The beam from a laser range finder is scanned across a surface using either

- Standard pan tilt unit
- Pan rotating prism unit
- Pan rotating mirror

Pan Rotating Prism Unit

The fast scan axis is implemented by rotating a multi faceted prismatic mirror as shown in the diagram, with this the slow scan axis is implemented by rotating the whole prism scanner module. As with the previous method, range, amplitude or both are logged to produce an image.

High resolution, high accuracy images require many minutes or even hours to construct.

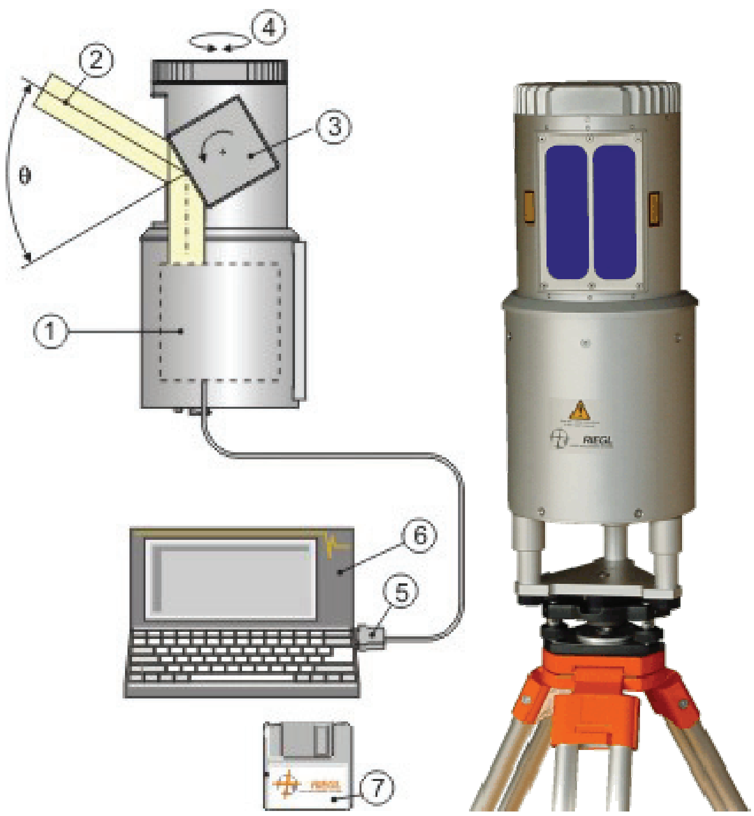

Figure 6.2: Pan prism scanner

1. **Laser Range Finder**
2. **Beam**
3. **Scanned Prismatic Mirror**
4. **Pan Axis**
5. **External Interface**
6. **Display Computer**
7. **Display Software**

Rotating Mirror Scanner

One of the most common imaging systems used in robotics is the SICK laser scanner, an example of which is shown in the figure below.

Figure 6.3: SICK laser scanner unit

The dismantled SICK laser shown in the photographs uses a single mirror mounted on the motor shaft at an angle of 45° to the fixed laser-beam axis to produce a scanned beam.

A mirror behind the laser diode collects the received energy and focuses it onto the receiver diode.

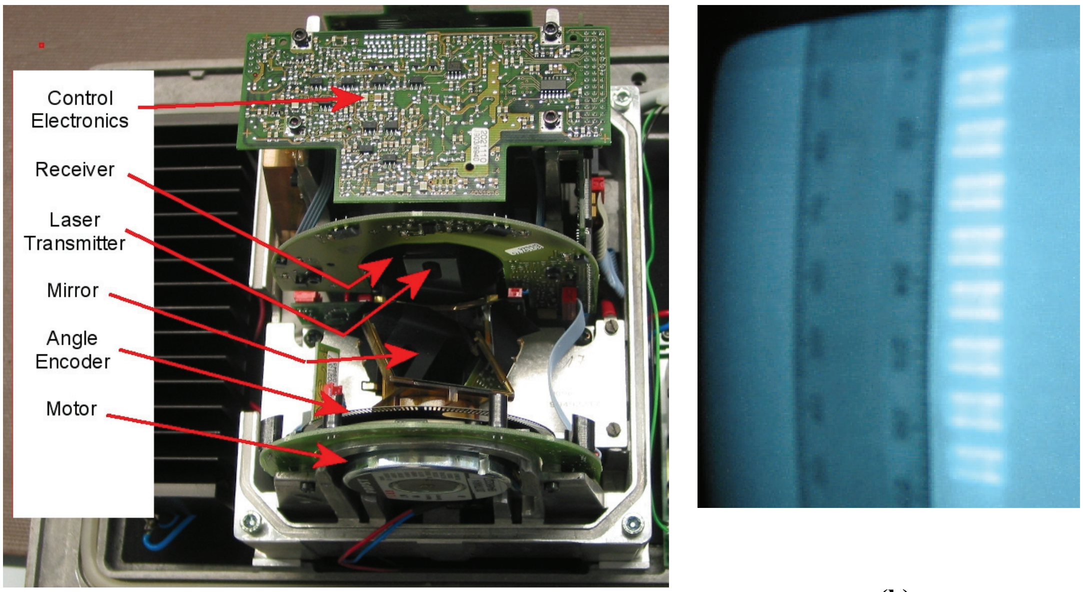

(a) **(b)**

Figure 6.4: Photographs showing (a) interior of a SICK laser unit and (b) an IR image of the laser pulses generated by the unit

6.2. Laser Radar Performance

6.2.1. The Laser Radar Range Equation

Referring to the geometry shown below, the signal power received by the laser range finder at range R is as follows:

$$S = \frac{P}{4\pi R^2} \cdot \frac{4\pi}{(\pi/4)\theta_{BW}^2} \cdot \frac{\pi}{4}\left(R\theta_{BW}\right)^2 . \rho . \frac{1}{2\pi R^2} . A . \tau_o \qquad (6.1)$$

(1) (2) (3) (4) (5) (6) (7)

where S – target signal power at the laser radar (W)
P – transmitted pulse power (W)
R – range to the target (m)
θ_{BW} – laser beamwidth (rad)
ρ - target backscattering coefficient
A – lens aperture area (m^2)
τ_o – optical efficiency

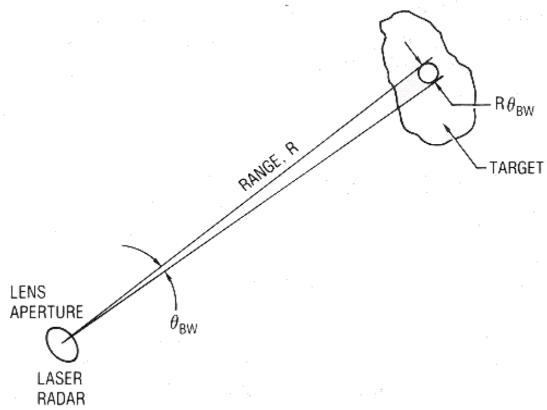

Figure 6.5: Laser radar target area

(1) Point source power over a spherical area $4\pi R^2$. The power of a point source without the benefit of a lens that focuses the power in a given direction.
(2) Measure of the focussing effect of the lens where it is used to direct the radiated power in a given direction. The gain is the ratio of the spread of the power over a sphere of 4π sr and the laser beamwidth in sr.
(3) The area of the target. In this case, the laser spot is smaller than the target area.
(4) The backscatter coefficient of the target. This depends on the material reflectivity and the surface roughness.
(5) The power from the target is scattered equally over the forward hemisphere of 2π sr. The resulting power density back at the laser will be $1/2\pi R^2$. An alternative is to use the Lambertian scattering assumption which is that the reflected flux per solid angle is proportional to the cosine of the angle between the normal to the surface and the reflection angle. In this case the spread is π.
(6) The target return power that is intercepted by a lens with area A.
(7) The optical efficiency of the laser radar transmission chain from the front aperture of the lens.

The formula can be simplified to the following for a spherical target power distribution.

$$S = \frac{PA\tau_o \rho}{\pi R^2} \text{ W.} \tag{6.2}$$

If the laser beam is larger than the target size, then term (3) should be substituted for by the laser radar cross-section σ and the equation becomes.

$$S = \frac{2PA\sigma\tau_o}{\pi^2 R^4 \theta_{BW}^2} \text{ W,} \tag{6.3}$$

where: θ_{BW} - λ/D,
λ - Wavelength (m),
D – Lens diameter (m),

In contrast to the 3dB half-power beamwidth definition used in microwave radar analysis. In optical systems the 1/e=0.367 level is used which equates to a beamwidth of $1.05\lambda/D$, where D is the lens diameter.

Substituting for θ_{BW} in terms of the lens area and the wavelength

$$\theta_{BW}{}^2 = \frac{\lambda^2}{D^2} = \frac{\lambda^2 \pi}{4A}. \tag{6.4}$$

The final equation is

$$S = \frac{8PA^2\sigma\tau_o}{\pi^3 R^4 \lambda^2} \text{ W.} \tag{6.5}$$

6.2.2. Laser Receivers

Direct detection laser receivers convert the echo directly into a voltage or current using PIN or Avalanche photodiodes. Heterodyne receivers down-convert the received signal to a lower frequency by mixing with the output of a stable local oscillator. The signal can then be amplified and filtered to enhance the detection process. Because phase information is maintained, such receivers can be used to measure speed by Doppler processing.

Direct Detection

The detector noise for direct detection is given by

$$N = \frac{(A_d \Delta f)^{1/2}}{D^*} \text{ W,} \tag{6.6}$$

where: N – Noise level (W),
A_d – Detector area (cm^2),
Δf – Receiver bandwidth (Hz),
D^* - Detectivity ($cm\text{-}Hz^{1/2}W^{-1}$).

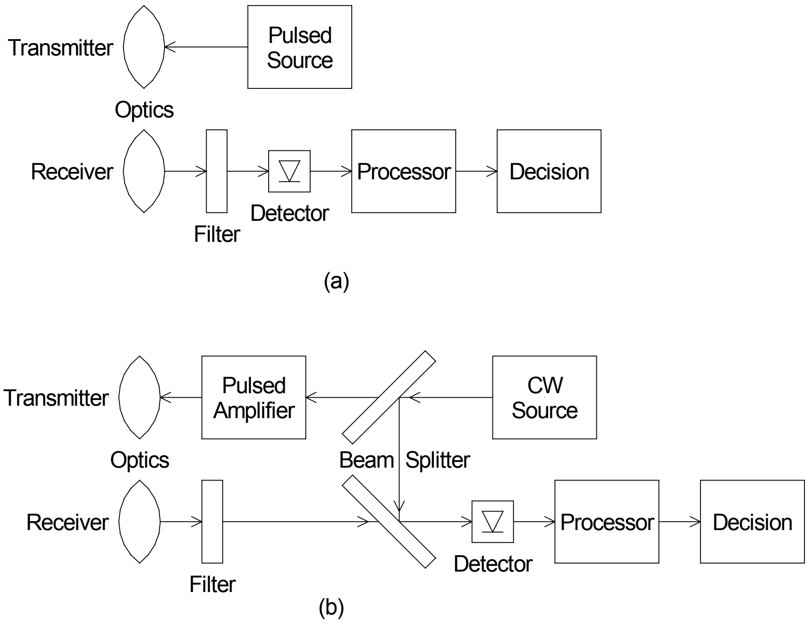

Figure 6.6: Laser receivers using (a) direct detection and (b) heterodyne techniques

The detector area for a square detector is related to the lens diameter and the focal length as follows

$$A_d = \left(\alpha_d^{1/2} f_1\right)^2 = \alpha_d f_1^2 , \tag{6.7}$$

where A_d – Detector area (cm^2),
$\alpha_d^{1/2}$ - Instantaneous detector field of view (IFOV).

The focal length f_1 can be written as the product of the lens diameter (D) and the lens focal number (f/#)

$$f_1 = (f/\#)D . \tag{6.8}$$

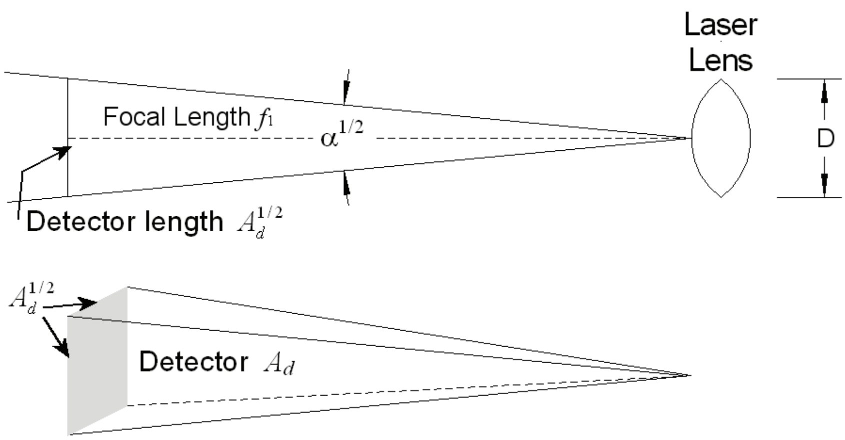

Figure 6.7: Detector area relationship to focal length

Direct Detection Photodiodes

A p-n diode's deficiencies are related to the fact that the depletion area (active detection area) is small and many electron-hole pairs recombine before they can create a current in the external circuit. In the PIN photodiode, the depleted region is made as large as possible. A lightly doped intrinsic layer separates the more heavily doped p-types and n-types. The diode's name comes from the layering of these materials positive, intrinsic, negative — PIN. Figure a below shows the cross-section and operation of a PIN photodiode. The conversion efficiency of these devices is between 0.5 and 1 A/W of incident power.

The avalanche photodiode (APD) operates as the primary carriers, the free electrons and holes created by absorbed photons, accelerate, gaining several electron Volts of kinetic energy. A collision of these fast carriers with neutral atoms causes the accelerated carriers to use some of their own energy to help the bound electrons break out of the valence shell. Free electron-hole pairs, called secondary carriers, appear.

Collision ionisation is the name for the process that creates these secondary carriers. As primary carriers create secondary carriers, the secondary carriers themselves accelerate and create new carriers. Collectively, this process is known as photomultiplication. Typical multiplication ranges in the tens and hundreds. For example, a multiplication factor of eighty means that, on average, eighty external electrons flow for every photon of light absorbed.

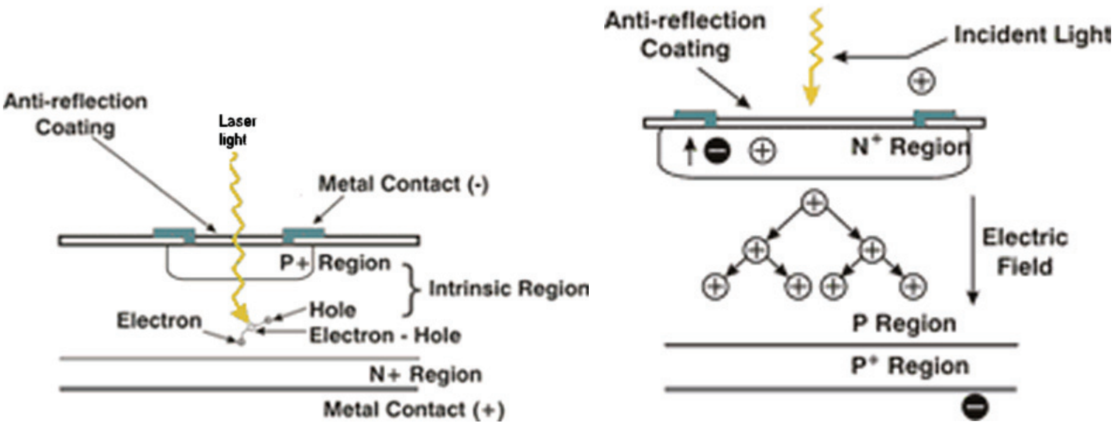

(a) **(b)**

Figure 6.8: PIN (a) and (b) avalanche photodiode (APD) operational principles

APDs require high-voltage power supplies for their operation. The voltage can range from 30 or 70 Volts for InGaAs APDs to over 300 Volts for Si APDs. This adds circuit complexity. Also, APDs are very temperature sensitive, further complicating circuit requirements. Because of the added circuit complexity and the high voltages that the parts are subjected to, APDs are always less reliable than PIN detectors.

The conversion efficiency of typical APDs varies between 0.5 and 100 A/W.

Heterodyne Detection

The noise spectral density of an ideal amplifier is given by the following formula:

$$\psi(f) = \frac{hf}{e^{hf/kT} - 1} + hf \quad \text{W/Hz,} \tag{6.9}$$

where: *Ψ(f)* – Spectral density (W/Hz),
h – Plank's Constant 6.6256×10^{-34} (Ws^2),
f – Frequency (Hz),
k – Boltzmann Constant 1.38×10^{-23} (Ws/K),
T – Absolute Temperature (K).

Substituting for the wavelength $\lambda = c/f$ and plotting in the figure below. Also plotted is $\mu(f) = hf$ and $\gamma(f) = kT$.

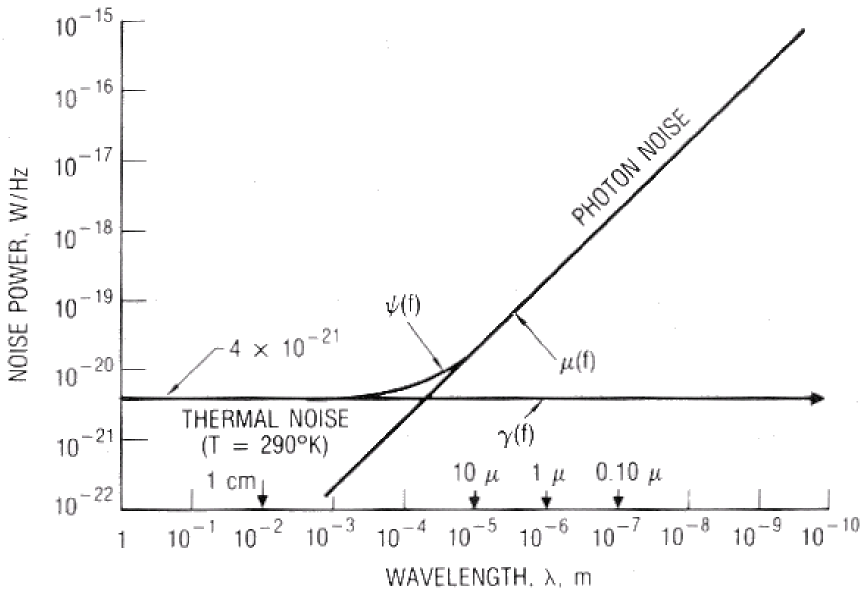

Figure 6.9: Laser radar noise floor as a function of wavelength for heterodyne detection

For microwave radars the noise power density is determined by the thermal noise floor and is approximately $\gamma(f) = kT$ while in the infrared, the noise power density is determined by the photon noise $\mu(f) = hf$.

The noise level of an heterodyne receiver can therefore be written as follows:

$$N = \frac{hfB}{\eta} \quad \text{W,} \tag{6.10}$$

where: η - Quantum efficiency (0.3 to 0.5) (how many photons are required to produce one photo-electron),
B – Receiver bandwidth (Hz).

It is easy to show that at 290K, the noise floor for a microwave receiver is about 10dB lower than a photon noise limited laser receiver operating at 10.6µm with a 50% quantum efficiency.

6.2.3. Signal to Noise Ratio and Detection Probability

Glint targets represent returns from corner reflectors or normal surfaces (such as the ground) where there is a single dominant scatterer. Returns are normally fairly constant from pulse to pulse.

Using the signal to noise ratio for a glint target calculated using the formulae derived above, the detection probability P_d and false alarm probability P_{fa} can be determined from the graph below which give the probability of detecting a sinusoidal signal of constant magnitude in Gaussian noise.

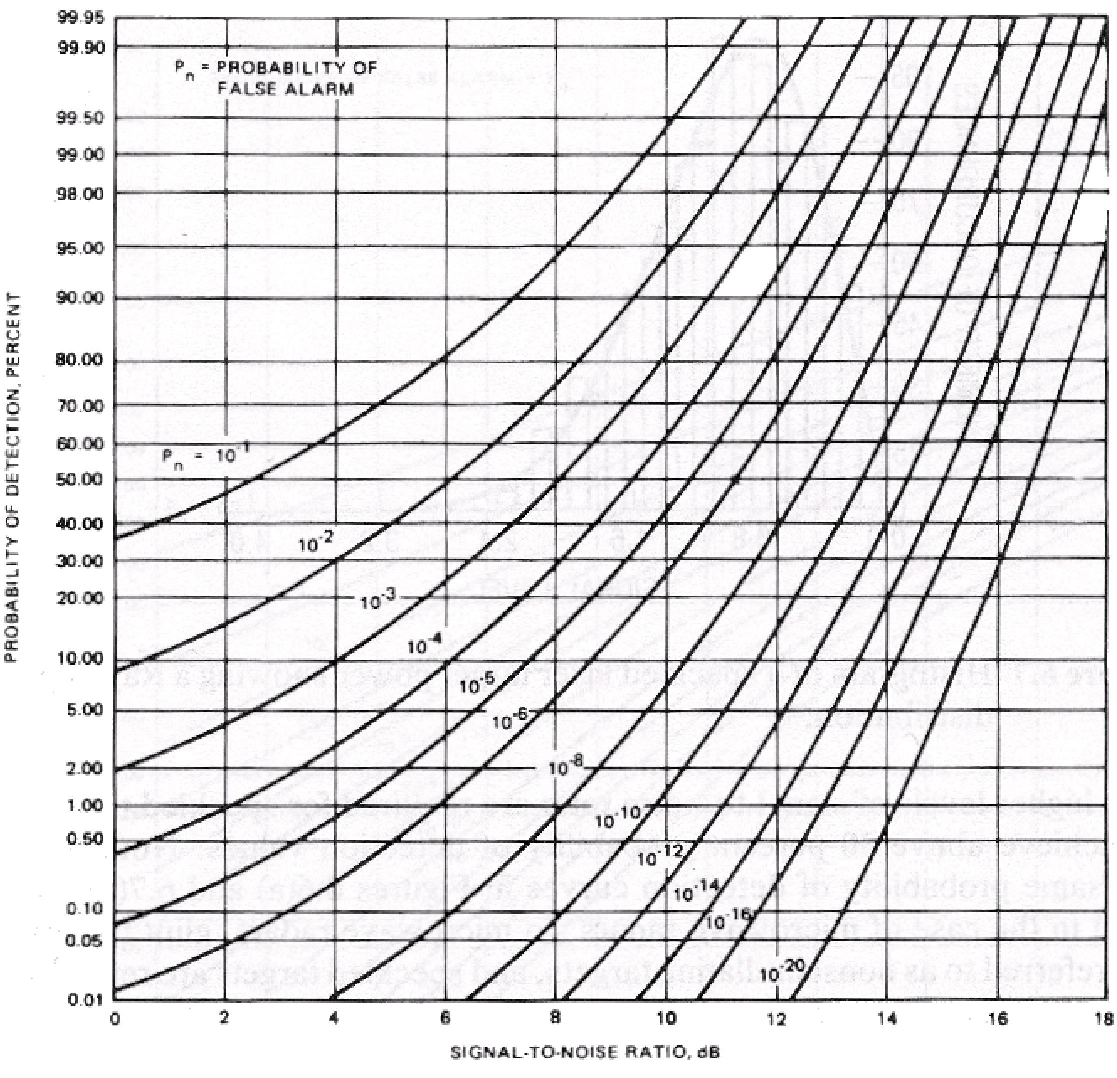

Figure 6.10: Probability of detection of a LIDAR for fluctuating targets

6.2.4. Example of a Laser Radar

An earth bound CO_2 laser operating at a wavelength of 10.6μm radiates through a collimating lens with a diameter of 500mm. If it produces 500W pulses each of duration 0.1s answer the following questions.

Mean distance to the moon is 384400km

The power is $P_{dB} = 10\log_{10}(500) = 27$dBW

The $1/e$ beamwidth is:

$$\theta_{BW} = \frac{1.05\times\lambda}{D} = \frac{1.05\times 10.6\times 10^{-6}}{0.5} = 22.3\mu rad$$

The antenna aperture is

$A = \pi D^2/4 = 0.196$ m^2

a) What would the diameter of the footprint be on the moon

$d = R\theta_{BW} = 3.844\times 10^8 \text{x} 22.3\times 10^{-6} = 8556$m

The area of the footprint on the moon is

$A_{foot} = \pi d^2/4 = 57.5\times 10^6$ m^2 [77.6dBm^2]

b) Ignoring atmospheric effects what would the power density on the moon be in W/m^2

$S_I = P/A_{foot} = 500/57.5\times 10^6 = 8.7\mu$W/m^2

$S_i = P_{dB} - A_{foot} = 27\text{-}77.6 = -50.6$dBW/m^2

c) A retro-reflector with a diameter of 10cm and a reflectivity of 0.99 reflects some of the power back to earth. What is the received power density.

The effective cross section of the retro-reflector is (see Chapter 9)

$$\sigma = 0.99\frac{4\pi D^4}{3\lambda^2} = 0.99\frac{4\pi\times 0.1^4}{3\times\left(10.6\times 10^{-6}\right)^2} = 3.7\times 10^6 m^2 = 65.7dBm^2$$

The power density back on the earth is given by the following formula

$$S_R = \frac{2P\sigma}{\pi^2 R^4\theta_{BW}^2} = \frac{2\times 500\times 3.7\times 10^6}{\pi^2\times\left(3.844\times 10^8\right)^4\left(22.3\times 10^{-6}\right)^2} = 3.45\times 10^{-17} W/m^2$$

d) Is the reflected power density from the moons surface back on the earth (backscatter coefficient 0.2) larger or smaller than that returned by the retro-reflector.

The power density back on earth is just

$$S_R = \frac{P\rho}{\pi R^2} = \frac{500 \times 0.2}{\pi \left(3.844 \times 10^8\right)^2} = 2.15 \times 10^{-16} W/m^2$$

Which is 10× higher than that received from the corner reflector

e) If an heterodyne receiver uses the same size lens, what is the single pulse signal to noise ratio that we could expect

For a receiver bandwidth matched to the pulsewidth $\beta = 1/\tau = 10$Hz, and a quantum efficiency $\eta = 0.5$

$$N = \frac{hf\beta}{\eta} = \frac{hc\beta}{\eta\lambda} = \frac{6.625 \times 10^{-34} \times 3 \times 10^8 \times 10}{0.5 \times 10.6 \times 10^{-6}} = 3.75 \times 10^{-19} W$$

Assuming that the optical efficiency is 100%, the received power is the product of the power density and the receive aperture

$S = S_R A = 2.15\times10^{-16}\times0.196 = 4.21\times10^{-17}$ W

The single pulse signal to noise ratio is, S/N = 112 (20.5dB)

6.3. Digital Terrain Models

Laser altimeters measure height by transmitting a narrow pulse of IR radiation in a narrow beam towards the ground. Because the ground is rough (compared to the wavelength of the light), the laser pulse is generally scattered in all directions including back up to the aircraft.

Both the roundtrip time and the amplitude of the received echo can be logged, and by using the push-broom technique, discussed earlier, strip-map images of the ground can be generated. Because the swathe painted on the ground is quite narrow (it depends on the height and the scan angle), it is generally necessary to produce composite images produced by successive passes over adjacent, overlapping areas.

To produce well registered, accurate images, the aircraft position is logged using a combination of GPS and inertial navigation systems. Using this technique, the position of a spot on the ground can be determined in this way to an accuracy of 10cm (vertically) and 50cm (horizontally).

6.3.1. Surface Models

A digital image is a rectangular array of cells where each cell contains a single value.

- A topological image is produced if the height information is used
- A reflectivity image is produced if the echo amplitude information is used.

Though the points measured on the ground usually have a non-linear spacing, the cells in the image are spaced regularly (using interpolation) to facilitate processing.

A digital elevation model (DEM) is a continuous mathematical representation describing the shape of the surface where elevation is a function of longitude and latitude.

- Digital surface models (DSM) contain elevation values of the air/surface interface, it includes trees and buildings etc.
- Digital terrain models (DTM) reflect pure terrain information as it is represented on contour maps. These are produced by filtering the DSM information.

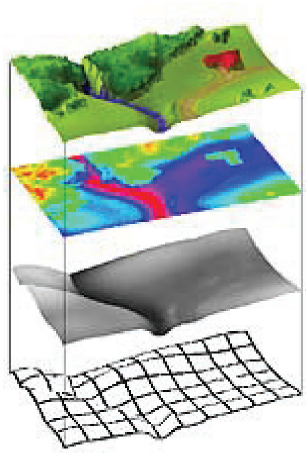

Figure 6.11: Digital model representations

6.3.2. Digital Landscapes

Digital landscapes are DSMs with additional information like surface colour and texture or vegetation types to allow a more realistic representation to be produced. Both DEMs and DSMs are considered to be 2½ -D representations of the earth's surface because only a single elevation value is given for each point on the surface, whereas in reality each point may have a multitude of surfaces (tree canopy, building roof and ground).

If the fine structure of the pulse echo is examined, it yields information about the vertical structure of the surface, roughness, height and shape of manmade objects can be determined as well as canopy density and height of trees. In addition the reflectivity properties can be analysed to produce images similar to those available from infrared cameras (albeit with lower resolution)

6.3.3. Combining Image Types

The usual approach in commercial systems is to use high resolution digital camera in parallel with the laser altimeter. This has the advantage of producing a higher resolution image, and the ability to image across different spectral bands. However, unlike the laser images, it required an external source of illumination which will probably be at an angle to the camera and thus produce shadows.

This first image shows a transformed topological image produced by the scanning laser system. It is possible to see that this image has been manipulated to include shadows which would not occur in the original image which is produced from directly above.

Figure 6.12: Transformed topological image

Individual buildings are resolved to an accuracy of 0.5 to 2m which is sufficiently good to resolve the heights, footprints and even the roof shapes of most buildings.

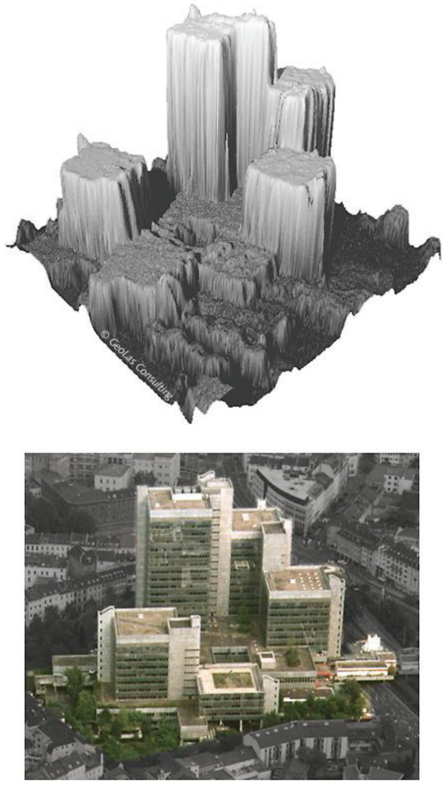

Figure 6.13: Topology image of a cluster of buidings

The high vertical accuracy available from a digital surface model allows simulations of flooding to be conducted. The following image shows the effect of the Rhine's flooding on the city of Bonn.

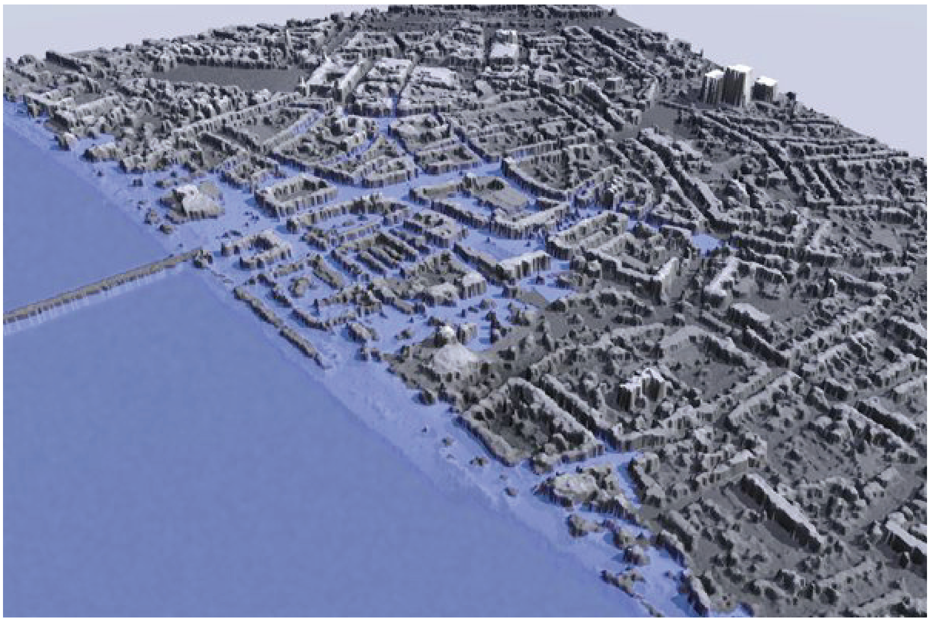

Figure 6.14: Application of topological images for flood analysis

6.4. Laser Based Sea-Bottom Profiling

The imaging principles developed for ground mapping can be extended to include sub-sea mapping as shown in the image generated using the Laser Airborne Depth Sounder (LADS) system

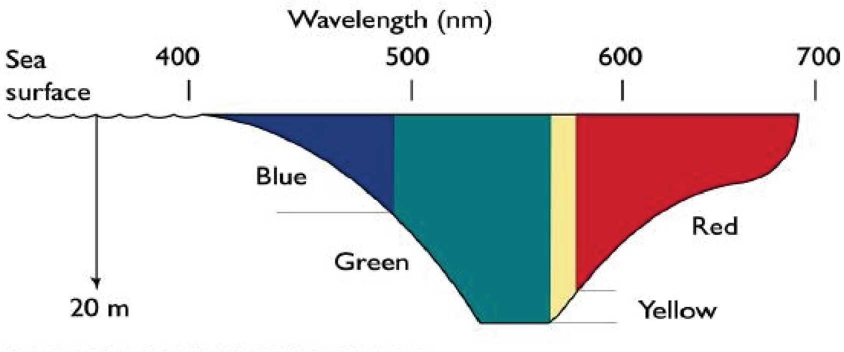

Figure 6.15: Inshore water penetration by light of different colours

Differential GPS and INS are used together to pinpoint the position of the aircraft while a laser altimeter measures the height of the aircraft above the sea and a scanned blue-green laser with good water penetration characteristics measures the height of the aircraft above the sea bottom across a swathe

The process can produce depth information at a rate of 64 square km per hour with a spatial resolution of 5m.

- Sounding rate 900Hz
- Water depth between 0.5 and 70m
- Swath width 240m
- Resolution normally 5×5m but with a 2×2m option
- Position accuracy 5m CEP 95%

Areas of cloud cover or high water turbidity that could compromise the performance of the LADS system are identified using satellite images provided by NOAA, and those areas are avoided during the survey.

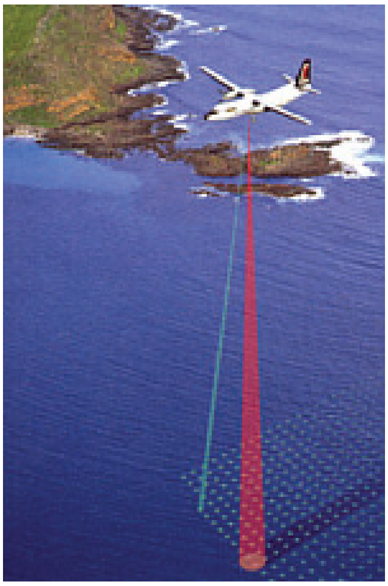

Figure 6.16: Laser based sea bottom profiling

The Royal Australian Navy's Laser Airborne Depth Sounder (LADS), mounted on a Fokker F27-500 performed a survey of Sydney Harbour in May 2002 as illustrated in the figure below.

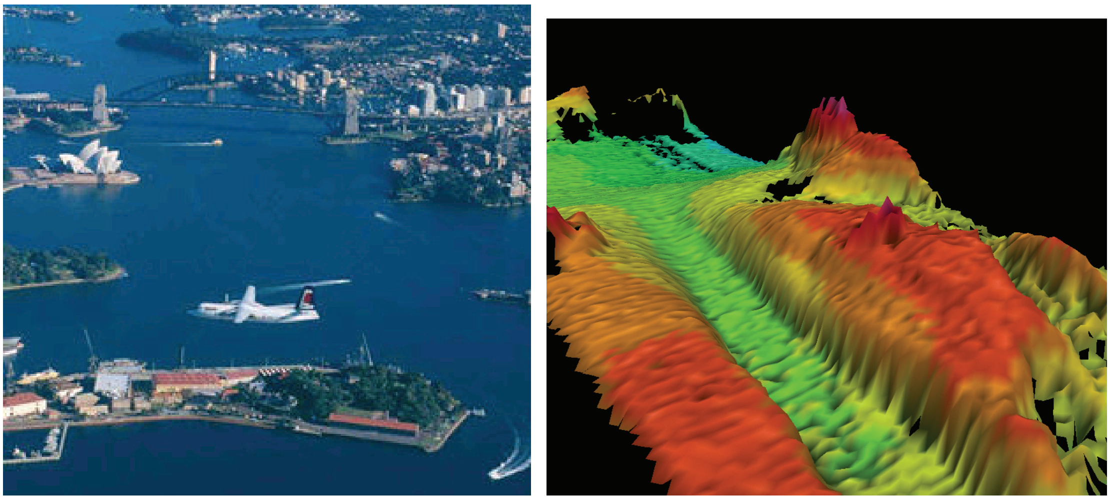

(a) (b)

Figure 6.17: LADS Survey of Sydney Harbour showing (a) the aircraft and (b) the sow and pigs reef and the western channel

6.5. 2D Laser Scanners

Unlike the process shown above that relies on the forward motion of the vehicle to scan the one axis, 2D scanners involve scanning the laser range-finder using a raster to cover both elevation and azimuth angles as discussed.

With most scanners that operate over reasonably long ranges, the fast axis is usually scanned using a spinning mirror or prism, while the slow axis is scanned by rotating the whole scanner head.

This principle was used by Riegl to produce the range colour coded images shown below.

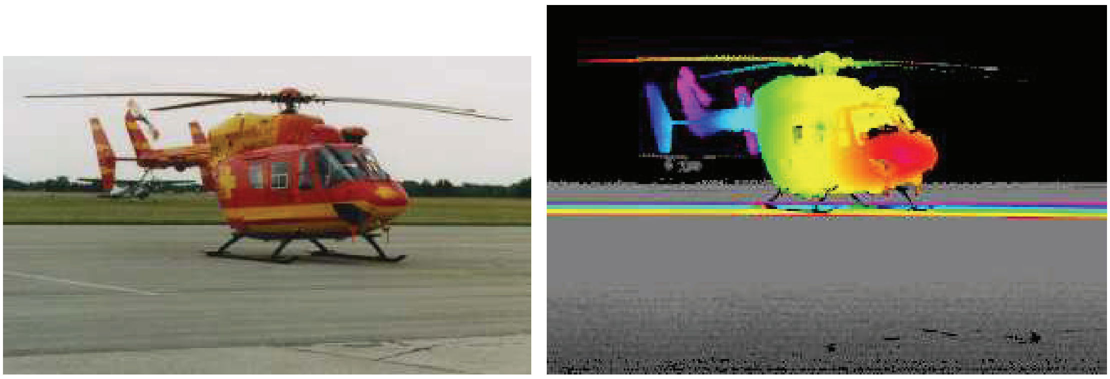

(a) (b)

Figure 6.18: 2D laser scanner colour coded images

6.6. 3D laser Scanners

The availability of low cost high resolution laser scanners has lead to a proliferation of industrial applications from volume estimation, architectural reproduction to CAD/CAM manufacturing.

For example, to determine its volume, the object is scanned from a number of carefully surveyed positions to produce individual views that are combined to generate a complete image point cloud image. Surface heights on a regular grid are computed from the point cloud data and the volume is calculated by integrating the height of the grid over the surface.

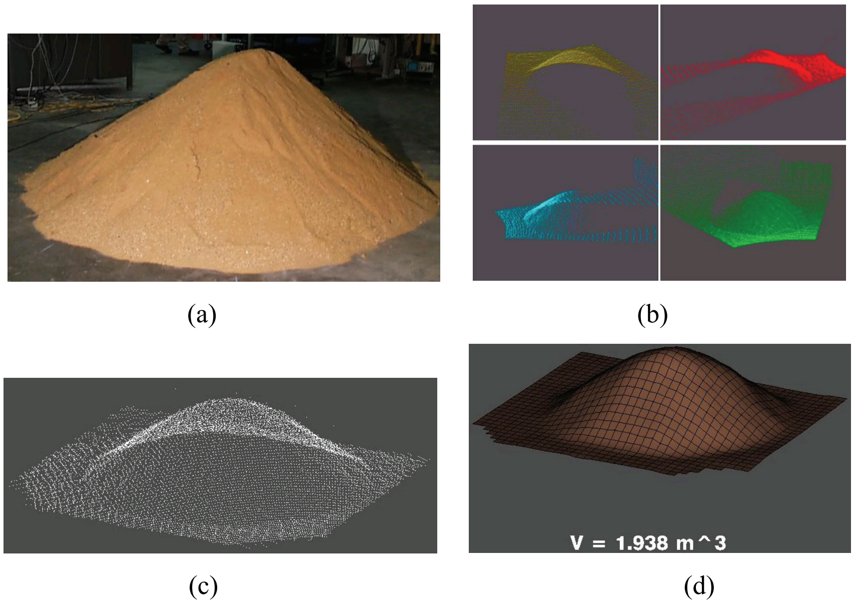

Figure 6.19: Process of estimating volume using a 3D laser scanner

In the CAD/CAM application, a component is scanned in a similar manner to produce a point cloud image which is then further processed to produce 3D digitised data of the surface. This is then used to reproduce the original component using a “rapid prototyping printer” or a CNC machine.

Figure 6.20: High resolution laser scanner produces a 3D model for computer aided manufacture

6.7. 3D Millimetre Wave Radar Scanners

Under adverse weather conditions or through dust or smoke, the performance of laser systems is degraded due to absorption and scattering (see Chapter 8). An alternative, albeit one with poorer angular resolution, is to use a millimetre wave radar to produce images.

Millimetre wave frequencies are used because their wavelength is sufficiently long compared to the sizes of dust, smoke or mist that the signal is hardly attenuated. Scanners based on standard pan-tilt technology (slow), or moving mirror (fast) have been developed at the ACFR.

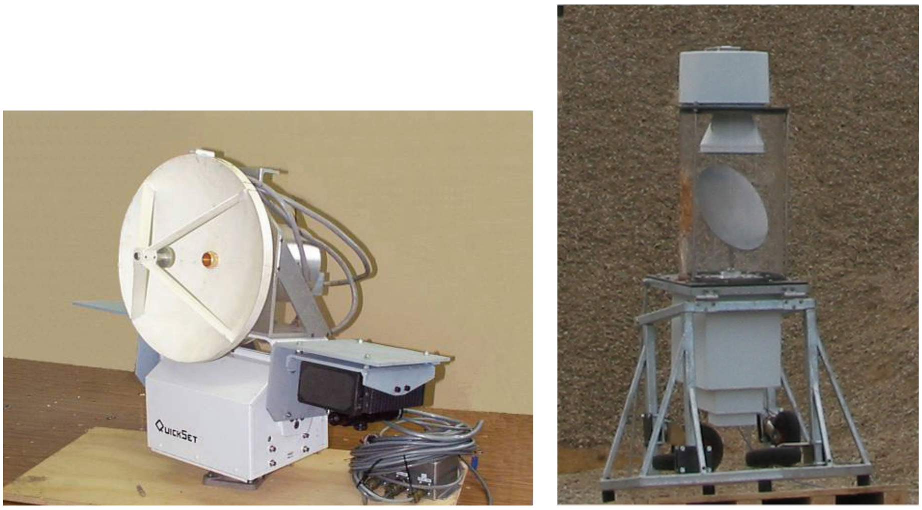

Figure 6.21: Millimetre wave radar imagers based on (a) pan and tilt and (b) mirror scanner

In addition to being relatively immune to weather conditions, because of the wide beamwidth, data produced by radar scanners can illuminate multiple targets simultaneously. This allows the unit to "see" through trees and to obtain foliage density information

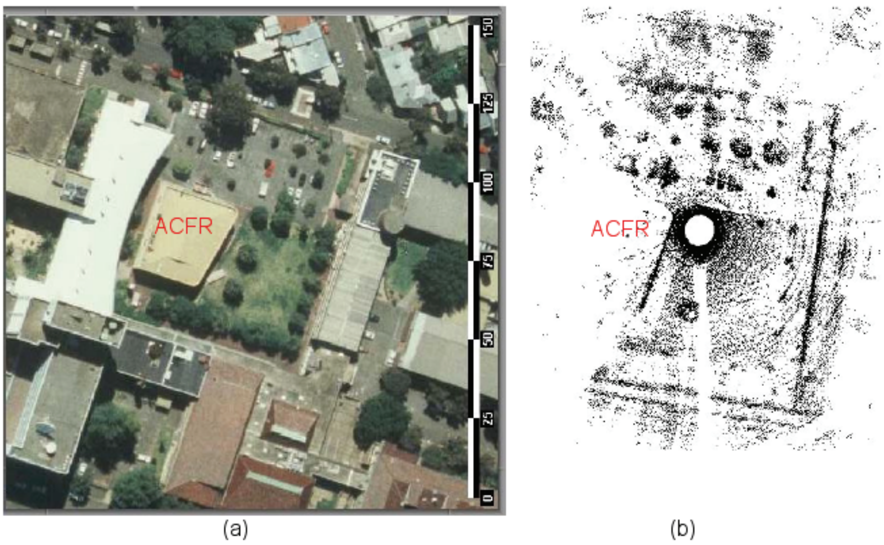

Figure 6.22: Radar image and photograph of the ACFR and surrounds - plan view

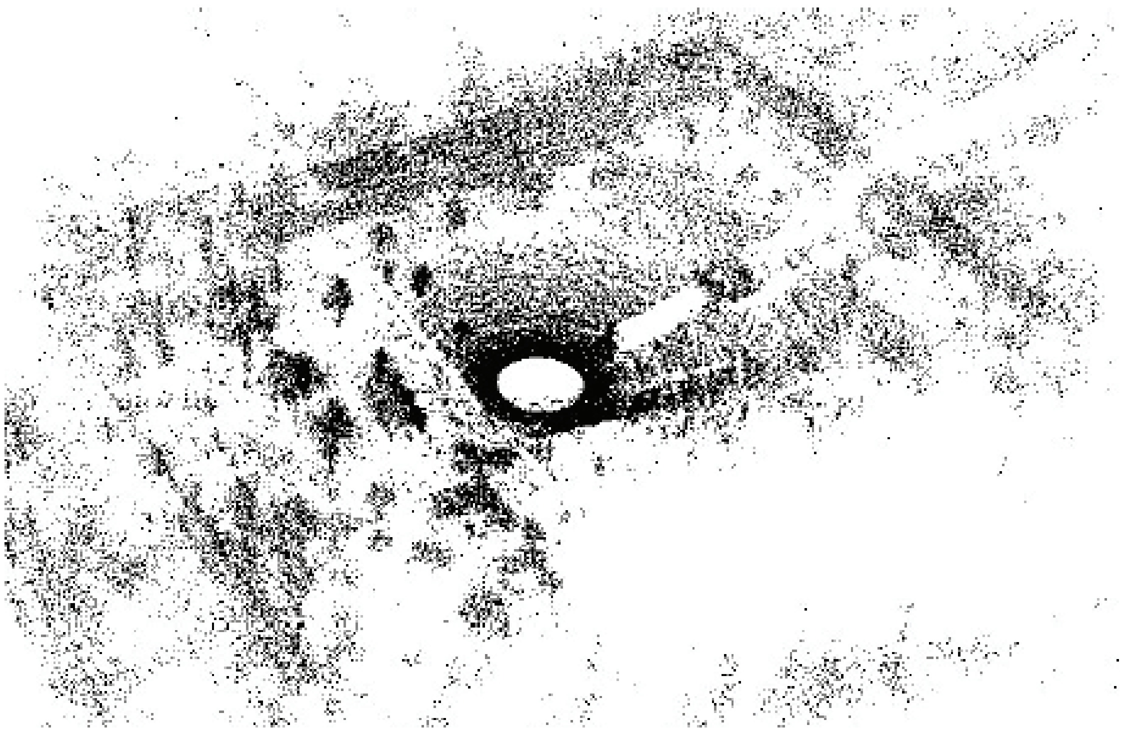

Figure 6.23: Radar image of the quad adjacent to the ACFR – 3D perspective view

6.8. Scanning Acoustic Microscopes

The Scanning Acoustic Microscope (SAM) produces images by scanning a focussed beam of acoustic energy (sound) across a sample to measure its elastic properties

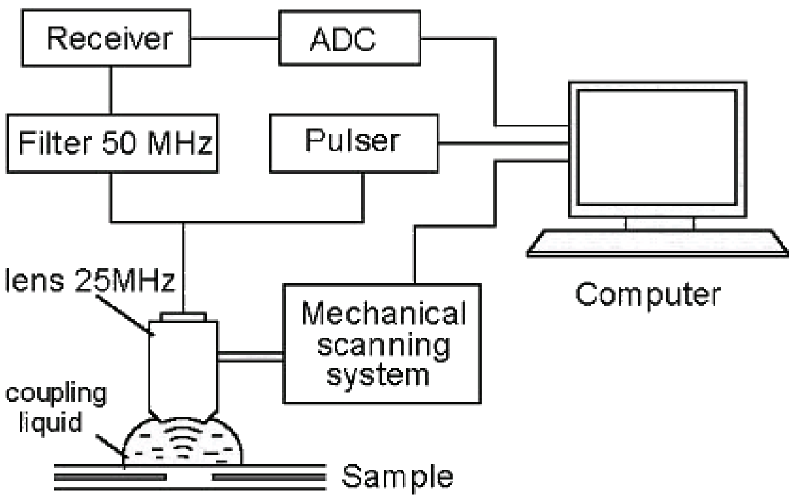

Figure 6.24: Schematic diagram showing the components of a scanning acoustic microscope

In principle this process is very similar to that used by the medical ultrasound scanning technology discussed in Chapter 12. The primary difference in this application is the use of mechanical scanning techniques while most medical systems use electronic scanning through one plane.

6.8.1. The Acoustic Lens

The principles involved are similar to those of an optical microscope, that is, different propagation velocities through different media are used to focus a beam so as to resolve small objects

Unlike its optical counterpart, where the relative velocities between the two media seldom exceeds 1.9 (the refractive index difference), with the acoustic microscope, the velocity can decrease by a factor of 10 or more when traversing a suitable solid-liquid interface.

A suitable lens such as the one manufactured for the original Stanford University microscope consisted of a concave spherical sapphire lens with a radius of approximately 40μm immersed in water.

At the interface, the sound waves are bent sharply inward as they encounter the liquid, to focus close to the centre of curvature of the sphere.

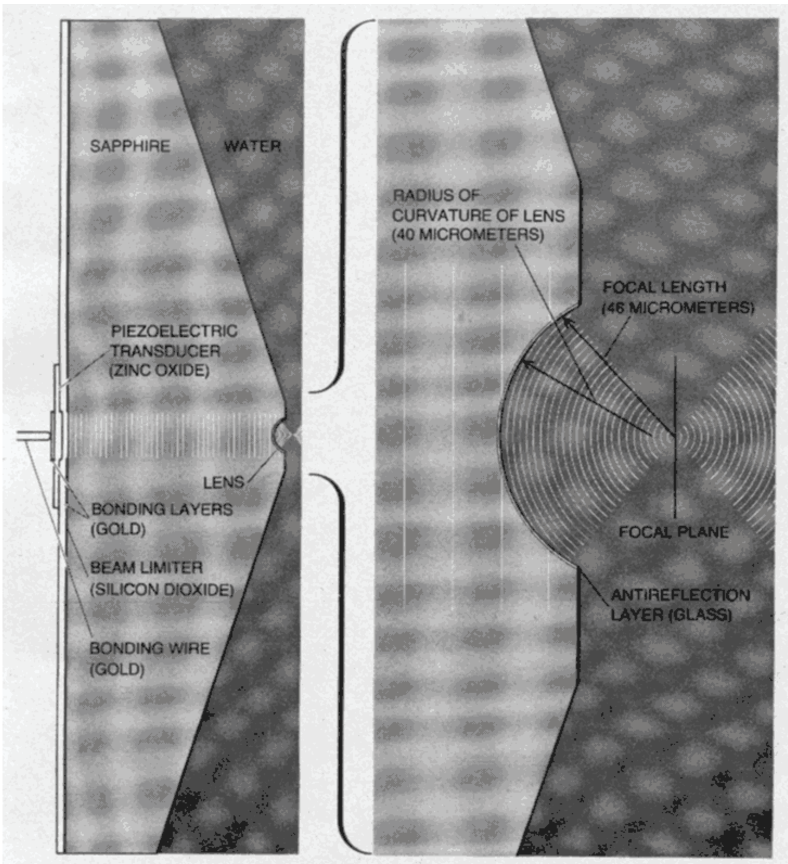

Figure 6.25: Schematic diagram of an acoustic lens

The first step in the imaging process is to convert the high frequency electrical signal to an acoustic one by means of a piezoelectric film deposited on the back of the sapphire lens. This generates an acoustic wave that travels across the lens material until it strikes the back of the curved section where the focussing takes place.

The different elastic properties of the material distort the phase of the signal reflected from the focal point which then follow the reverse path and are detected by the same piezoelectric film which acts as a microphone.

Modern SAMs use short ultrasound pulses at a frequency ranging between 15 and 180MHz to separate the received and transmitted signals as well as time gating to image specific depths in the medium.

6.8.2. The Scanning Mechanism

An image is formed by scanning the focal point across the object in a raster fashion, storing the amplitude of the received signal along with the spatial co-ordinates and then displaying the complete picture. In the original microscopes as shown in the figure below this process could take a couple of seconds.

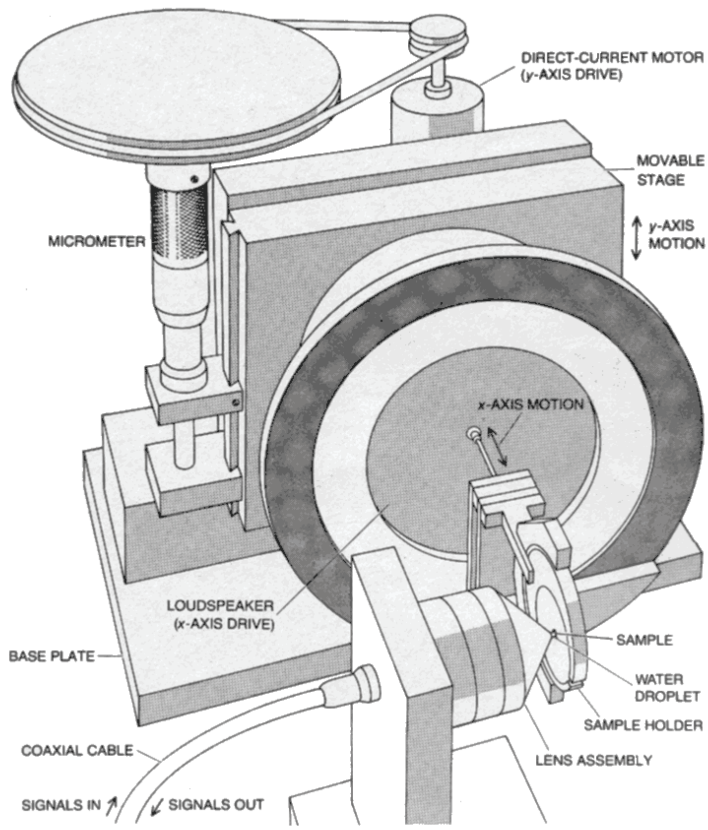

Figure 6.26: Schematic diagram of the scanning mechanism of an early SAM.

The original SAM, shown in the figure used a loudspeaker moving driven at 60Hz for the horizontal translation stage, and a DC servo motor driving a micrometer for vertical translation. An image was formed by synchronising this raster scan with a TV monitor the intensity of which was controlled by the amplitude of the reflected acoustic signal.

With more modern microscopes based on commercial scanning probe microscope (SPM) technology, the process is much faster.

6.8.3. Images

Because the process takes place in water which is compatible with living biological specimens, it is possible to make images of living cells. In the following example, however, the cell was fixed and stained so that a comparison could be made between the acoustic and optical images.

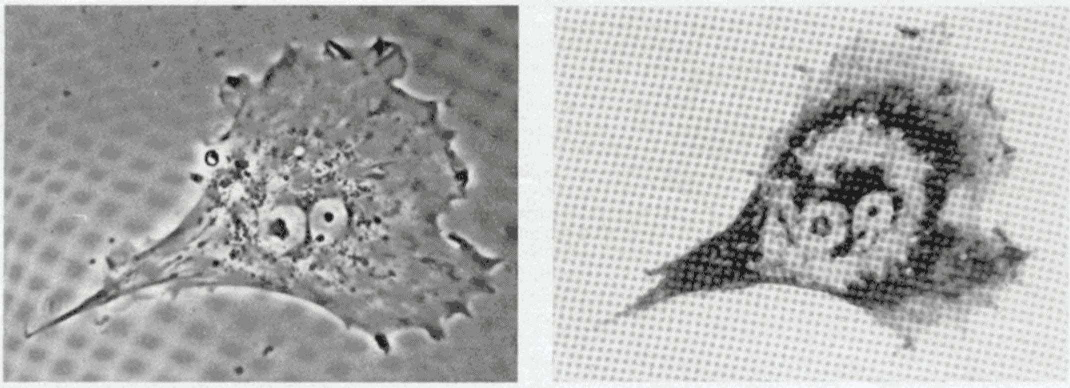

SINGLE CELL, a fibroblast cell obtained from the connective tissue of a chick embryo, is represented by an optical image (*left*) and a corresponding acoustic image (*right*). The cell was grown on a collagen-coated glass slide and was fixed with methanol by Randal N. Johnston of Stanford. Both micrographs reveal the network of internal fibers that holds the cell together. The contrast in the optical image results from a selective-staining technique; the contrast in the acoustic image results from variations in the elastic properties of structures in the cell. The fact that the acoustic technique works without staining suggests that it may be possible to visualize such structures in living cells.

Figure 6.27: Comparison of an acoustic image and an optical image of a single cell

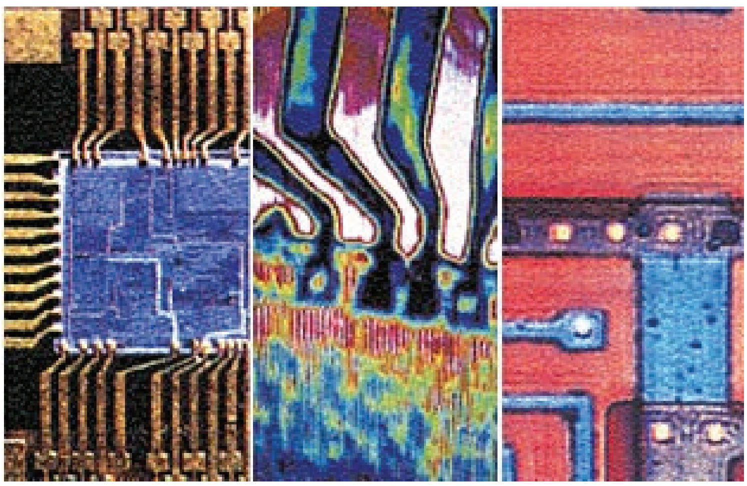

Figure 6.28: Acoustic images made of the interior of a potted IC. resolution increases from left

6.8.4. Near Field Microscopes

The scanning acoustic microscope has a limited resolution determined by the Rayleigh diffraction limit of the focussed beam.

To overcome this problem, the so-called near-field acoustic microscope was also developed using the fine mechanisms that have become available for (SPM's).

An acoustic wave is produced in the tiny area near the probe tip of the microscope (near-field area) and the interactions with the material are measured with a resolution that is not dependent on the wavelength.

6.8.5. Identification of Defects

During the propagation on the surface the surface acoustic wave interacts with the inhomogeneities like cracks, voids and topographic structures. Interference between the incident and reflected surface waves allows the detection of cracks that are an order of magnitude smaller than the spatial resolution of the microscope (approx. 1.5 µm at 1 GHz)

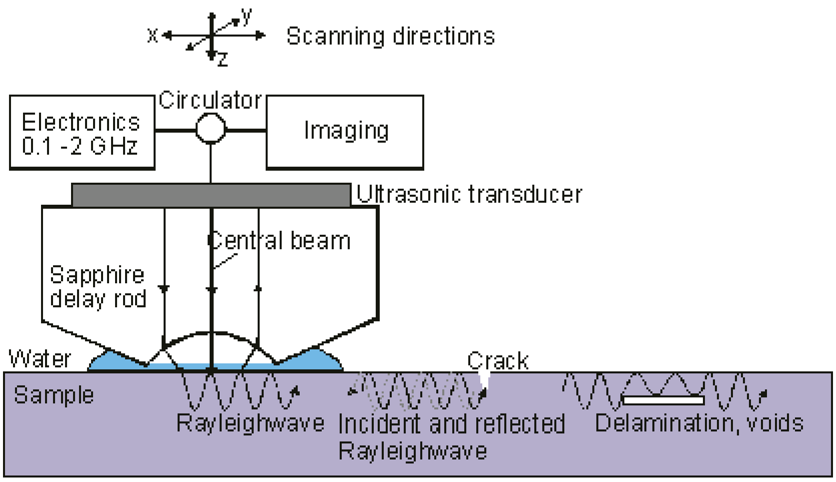

Figure 6.29: Mechanism to detect material defects using an acoustic microscope

6.9. References

[1] Imaging Laser Altimetry, http://www.geolas.com/Pages/laser.html, 28/02/2001.
[2] LADS, http://www.aims.gov.au/pages/facilities/remote_sensing/pages/rs_lads.html, 22/02/00.
[3] Depth Finder, *New Scientist,* 2 September 2000.
[4] S.Hovanessian, *Introduction to Sensor Systems,* Artech House, 1988.
[5] E. Brookner, *Radar Technology, Artech House, 1977.*
[6] M. Sinclair, *Laser Hydrography- Commercial Survey Operations*, Hydro 99,
[7] S. Scheding et. Al. *Terrain Imaging Millimetre Wave Radar.* ICARCV 2002, Singapore 2002.
[8] C.Quate, The Acoustic Microscope, Scientific American, October 1979
[9] Industrial Physicist "Seeing with Sound", www.aip.org/tip/INPHFA/vol-10/iss-3/p14.html
[10] Visualization and Volume Calculation of a Sand Pile by Laser Range Scanning (LIDAR), cic.nist.gov/lipman/sciviz/scan/
[11] Speed Up Your Production Projects and Save Money with 3D Laser Scanning, Digitzing and Reproduction Services by Cyber F/X ®, cyberfx.com/3d_laser_scanning.htm
[12] http://www.fiber-optics.info/articles/detector.htm
[13] Shallow Survey 2003, www.shallowsurvey.com/info_files/images3.html